Rotation of Polygonal Space Structures

C. Y. Wang and Layne T. Watson

TR 90-20

Rotation of Polygonal Space Structures

C.-Y. Wang
Departments of Mathematics and Mechanical Engineering
Michigan State University
East Lansing, MI 48824

Layne. T. Watson†
Department of Computer Science
Virginia Polytechnic Institute & State University
Blacksburg, VA 24061

Abstract. The free rotation in space of flexible polygonal structures about their axes is studied. The large deformation equations are formulated, resulting in a set of sixth order nonlinear differential equations. The governing parameter B represents the relative importance of centrifugal forces to flexural rigidity. Perturbation solutions are obtained for small B . The equations are also integrated numerically by quasi-Newton and homotopy methods. Forces, moments, and maximum deformations are determined for polygons of three to six sides and B up to 100. At very large B, the polygons deform into a circle.

1. Introduction. Space structures are much more flexible than their terrestrial counterparts [1] for the following reasons. Firstly, in order to minimize transportation weight, the structural members are made as thin and slender as possible. Secondly, the lack of gravitational pull allows designs of much lower rigidity than required by terrestrial standards. Thirdly, space structures in the foreseeable future are very large in size, measuring in kilometers. At the same time, space structures are often rotated, due to stability, thermal or artificial gravity requirements. This rotation induces centrifugal forces which deform the structural elements. Such deformations, whether large or small, may or may not be acceptable depending on the mission.

Previous literature on the deformations due to the rotation of flexible space structures include thin rods [2, 3] and rings [4, 5]. In this paper we shall consider the rotation of a polygonal frame in its own plane. In particular we are interested in the stresses and the large deformations caused by centrifugal forces.

2. Formulation. Figure 1a shows a polygonal frame of N sides, each side consisting of an originally straight elastic rod of length ℓ. The frame is rotated in its own plane about the center of gravity with angular velocity Ω. The rods may be rigidly joined, or they may be hinged together. In the latter case the polygonal shape is maintained only by rotation. In the limit as $N \to \infty$ the rigidly joined polygon becomes a circular elastic ring and the hinged joint polygon becomes a circular chain. Under rotation both cases are stable to small disturbances.

Let the origin of Cartesian axes (x', y') be at the center of mass and the x'-axis pass through one of the joints at point A (Figure 1b). Let s' be the arc length along the frame from that point.

† The work of L. T. Watson was supported in part by DOE Grant DE-FG05-88ER25068, NASA Grant NAG-1-1079, and AFOSR Grant 89-0497.

Due to symmetry the angle between the joints $2\pi/N$ is constant for all rotation rates. Thus we need to consider only the segment from $s' = 0$ to $s' = \ell/2$.

Let ds' be an elemental length whose distance from the origin is r' (Figure 1c). The centrifugal force on this elemental segment is

$$dF = \rho ds' \Omega^2 r', \tag{1}$$

where ρ is the mass per unit length of the rods. Now due to symmetry the force H' is normal to the x'-axis at point A. Thus the force components acting on the elemental length are

$$F_x = \int_0^{s'} \cos\phi \, dF, \tag{2}$$

$$F_y = \int_0^{s'} \sin\phi \, dF - H', \tag{3}$$

where ϕ is the angle of the distance vector r'. Let θ be the local angle of inclination of ds'. Then

$$x' = r' \cos\phi, \qquad y' = r' \sin\phi, \tag{4}$$

$$\frac{dx'}{ds'} = \cos\theta, \qquad \frac{dy'}{ds'} = \sin\theta. \tag{5}$$

A local moment balance on ds' gives

$$m + F_y ds' \cos\theta = m + dm + F_x ds' \sin\theta. \tag{6}$$

Furthermore, if the rods are slender enough, the local moment m is proportional to the local curvature:

$$m = EI \frac{d\theta}{ds'}, \tag{7}$$

where EI is the flexural rigidity. Equations (1)–(4), (6), (7) give

$$EI \frac{d^2\theta}{ds'^2} = \left[\int_0^{s'} \rho\Omega^2 y' \, ds' - H' \right] \cos\theta - \left[\int_0^{s'} \rho\Omega^2 x' \, ds' \right] \sin\theta. \tag{8}$$

Now normalize all lengths by ℓ, all forces by EI/ℓ^2 and drop primes. Equation (8) becomes

$$\frac{d^2\theta}{ds^2} = Y \cos\theta - X \sin\theta, \tag{9}$$

$$Y = B \int_0^s y \, ds - H, \qquad X = B \int_0^s x \, ds, \tag{10}$$

where $B \equiv \rho\Omega^2 \ell^4 / EI$ is a governing nondimensional parameter signifying the relative importance of centrifugal forces to flexural rigidity. It is more convenient to turn Equation (10) into differential form

$$\frac{dY}{ds} = By, \qquad \frac{dX}{ds} = Bx. \tag{11}$$

Equation (5) gives

$$\frac{dx}{ds} = \cos\theta, \qquad \frac{dy}{ds} = \sin\theta. \tag{12}$$

The boundary conditions are

$$x(0) = a, \qquad y(0) = 0, \tag{13}$$

$$X(0) = 0, \qquad Y(0) = -H, \tag{14}$$

$$y(1/2) = x(1/2)\tan(\pi/N), \qquad \theta(1/2) = \frac{\pi}{2} + \frac{\pi}{N}, \qquad \theta''(1/2) = 0, \tag{15}$$

plus either

$$\theta(0) = \frac{\pi}{2} + \frac{\pi}{N} \tag{16}$$

if the rods are rigidly joined, or

$$\theta'(0) = 0 \tag{17}$$

if the rods are hinged. There are eight boundary conditions for the sixth order equations (9), (11), (12) plus two unknowns a, H.

3. Small deformation solutions. The parameter B is small in the cases of small density, low rotation rates, short lengths or high flexural rigidity. Thus for small B the deformations are also small and we can perturb about the case when each element is straight. Let

$$\phi(s) = \phi_0(s) + B\phi_1(s) + \mathcal{O}(B^2), \tag{18}$$

where ϕ may be any of the dependent variables θ, X, Y, x, y or the unknowns H and a. The zeroth order solution is straightforward:

$$\theta_0 = \frac{\pi}{2} + \frac{\pi}{N}, \tag{19}$$

$$Y_0 = X_0 = 0, \tag{20}$$

$$x_0 = s\cos\left(\frac{\pi}{2} + \frac{\pi}{N}\right) + \frac{1}{2}\csc\left(\frac{\pi}{N}\right), \tag{21}$$

$$y_0 = s\sin\left(\frac{\pi}{2} + \frac{\pi}{N}\right), \tag{22}$$

$$H_0 = 0, \qquad a_0 = \frac{1}{2}\csc\left(\frac{\pi}{N}\right). \tag{23}$$

From Equations (9), (11), (12) the first order equations are

$$\frac{d^2\theta_1}{ds^2} = -Y_1\sin\left(\frac{\pi}{N}\right) - X_1\cos\left(\frac{\pi}{N}\right), \tag{24}$$

$$\frac{dX_1}{ds} = -s\sin\left(\frac{\pi}{N}\right) + \frac{1}{2}\csc\left(\frac{\pi}{N}\right), \tag{25}$$

$$\frac{dY_1}{ds} = s\cos\left(\frac{\pi}{N}\right), \tag{26}$$

$$\frac{dx_1}{ds} = -\theta_1\cos\left(\frac{\pi}{N}\right), \qquad \frac{dy_1}{ds} = -\theta_1\sin\left(\frac{\pi}{N}\right), \tag{27}$$

with the boundary conditions

$$x_1(0) = a_1, \quad y_1(0) = 0, \quad X_1(0) = 0, \quad Y_1(0) = -H_1, \tag{28}$$

$$y_1(1/2) = x_1(1/2)\tan(\pi/N), \qquad \theta_1(1/2) = 0, \qquad \theta_1''(1/2) = 0 \tag{29}$$

plus either

$$\theta_1(0) = 0 \tag{30}$$

or

$$\theta_1'(0) = 0. \tag{31}$$

Without going into the details the solution is

$$\theta_1 = \cot\left(\frac{\pi}{N}\right)\left(c_0 + c_1 s + \frac{1}{8}s^2 - \frac{1}{12}s^3\right), \tag{32}$$

$$X_1 = \frac{1}{2}\csc\left(\frac{\pi}{N}\right)s - \frac{1}{2}\sin\left(\frac{\pi}{N}\right)s^3, \tag{33}$$

$$Y_1 = -\frac{1}{4}\cot\left(\frac{\pi}{N}\right)\csc\left(\frac{\pi}{N}\right) + \frac{1}{2}\cos\left(\frac{\pi}{N}\right)s^2, \tag{34}$$

$$x_1 = -\cot\left(\frac{\pi}{N}\right)\cos\left(\frac{\pi}{N}\right)\left(c_0 + \frac{c_1}{2}s^2 + \frac{1}{24}s^3 - \frac{1}{48}s^4\right), \tag{35}$$

$$y_1 = -\cos\left(\frac{\pi}{N}\right)\left(c_0 + \frac{c_1}{2}s^2 + \frac{1}{24}s^3 - \frac{1}{48}s^4\right), \tag{36}$$

$$H_1 = -\frac{1}{4}\cot\left(\frac{\pi}{N}\right)\csc\left(\frac{\pi}{N}\right), \qquad a_1 = 0, \tag{37}$$

where for the rigidly joined case

$$c_0 = 0, \qquad c_1 = -\frac{1}{24} \tag{38}$$

and for the hinged case

$$c_0 = -\frac{1}{48}, \qquad c_1 = 0. \tag{39}$$

The following values measure the extent of the deformation. The force occurring at the joints is

$$H = \frac{1}{4}\cot\left(\frac{\pi}{N}\right)\csc\left(\frac{\pi}{N}\right)B + \mathcal{O}(B^2). \tag{40}$$

The distance from the center of mass to a joint is

$$a = \frac{1}{2}\csc\left(\frac{\pi}{N}\right) + \mathcal{O}(B^2). \tag{41}$$

The distance from the center of mass to the midpoint of an element is

$$r = \sqrt{(x(1/2))^2 + (y(1/2))^2} = \frac{1}{2}\cot\left(\frac{\pi}{N}\right) - B\cot\left(\frac{\pi}{N}\right)\left(\frac{c_0}{2} + \frac{c_1}{8} + \frac{1}{256}\right) + \mathcal{O}(B^2). \tag{42}$$

The normalized moment or curvature at the midpoint is

$$\theta'(1/2) = \cot\left(\frac{\pi}{N}\right)\left(c_1 + \frac{1}{16}\right)B + \mathcal{O}(B^2). \tag{43}$$

4. Numerical method. Numerical integration is necessary for large deformations or when B is not small. Define

$$v = \begin{pmatrix} a \\ -h \\ \theta'(0) \end{pmatrix}, \tag{44}$$

and let $x(s;v)$, $y(s;v)$, $X(s;v)$, $Y(s;v)$, $\theta(s;v)$ be the solution of the initial value problem given by Equations (9), (11), (12) with initial conditions given by Equations (13), (14), (16) (or (17)), and (44). Note that the original two-point boundary value problem Equations (9), (11)–(17) is equivalent to solving the nonlinear system of equations

$$F(v) = \begin{pmatrix} y\left(\frac{1}{2};v\right) - x\left(\frac{1}{2};v\right)\tan\left(\frac{\pi}{N}\right) \\ \theta\left(\frac{1}{2};v\right) - \left(\frac{\pi}{2} + \frac{\pi}{N}\right) \\ \theta''\left(\frac{1}{2};v\right) \end{pmatrix} = 0. \tag{45}$$

(The case corresponding to the initial condition $\theta'(0) = 0$ is handled similarly, using instead $v_3 = \theta(0)$.)

Algorithms for solving the nonlinear system (45) typically require partial derivatives $\partial F_i/\partial v_j$. Since $F(v)$ is defined implicitly by the solution of a nonlinear ordinary differential equation, these partials cannot be found analytically. Finite difference approximations could be used, but for the same amount of work as a central difference, the partials can be calculated to the same accuracy as $F(v)$. This is done as follows: let

$$Z = \left(x, y, X, Y, \theta, \theta', \frac{\partial x}{\partial v_k}, \frac{\partial y}{\partial v_k}, \frac{\partial X}{\partial v_k}, \frac{\partial Y}{\partial v_k}, \frac{\partial \theta}{\partial v_k}, \frac{\partial \theta'}{\partial v_k}\right) \tag{46}$$

and consider the first order system

$$\begin{aligned}
Z_1' &= \cos Z_5, \\
Z_2' &= \sin Z_5, \\
Z_3' &= BZ_1, \\
Z_4' &= BZ_2, \\
Z_5' &= Z_6, \\
Z_6' &= Z_4 \cos Z_5 - Z_3 \sin Z_5, \\
Z_7' &= -Z_{11} \sin Z_5, \\
Z_8' &= Z_{11} \cos Z_5, \\
Z_9' &= BZ_7, \\
Z_{10}' &= BZ_8, \\
Z_{11}' &= Z_{12}, \\
Z_{12}' &= \cos Z_5 \left(Z_{10} - Z_3 Z_{11}\right) - \sin Z_5 \left(Z_9 + Z_4 Z_{11}\right),
\end{aligned} \tag{47}$$

with initial value

$$Z(0) = \left(v_1, 0, 0, v_2, \left(\frac{\pi}{2} + \frac{\pi}{N}\right), v_3, \delta_{1k}, 0, 0, \delta_{2k}, 0, \delta_{3k}\right). \tag{48}$$

By solving this system three times, for $k = 1, 2, 3$, all the partial derivatives $\partial F_i/\partial v_j$ can be calculated, with an accuracy determined by the accuracy of the numerical solution to the above initial value problem.

The nonlinear system (45) is solved by a combination of quasi-Newton methods (as implemented in the software package MINPACK from Argonne National Laboratory [6]) and globally convergent homotopy methods (as implemented in HOMPACK [7]). The mathematical and algorithmic details of these methods have been described extensively elsewhere [8], [9], [10], and so will not be repeated here. A good description of the combination approach, similar to that used here, to a fluid mechanics problem is in Heruska, Watson, and Sankara [11]. Very briefly, the strategy is to use the globally convergent and robust homotopy method to get a few solutions, and then use the inexpensive (but only locally convergent) quasi-Newton method to generate many solutions as B is slowly varied.

For large N and large B the solution v changes very rapidly as a function of B ($\|\partial v/\partial B\|_\infty > 10^3$), making it very difficult and time-consuming to track the solutions as a function of B. Consequently we did not pursue the solutions beyond $B = 400$.

5. Results and discussion. For large N and/or large B, the frame approaches a circle. The asymptotic limits are

$$r \to \frac{N}{2\pi}, \quad a \to \frac{N}{2\pi}, \quad \theta' \to \frac{2\pi}{N}, \quad H \to \frac{BN^2}{4\pi^2}. \tag{49}$$

If the parameters were normalized with the total length $N\ell$ instead of the side length ℓ, the dependence on N would then be absent in Equation (49).

Figure 2 shows, for the hinged case, the distance r from the center of mass to the midpoint of an element as a function of the rotation parameter B. The value of r increases from its nonrotating value of $(1/2)\cot(\pi/N)$ to its asymptotic value $N/(2\pi)$. Our approximate formulas for small and large B compare well with numerical results in their respective regions of validity. Notice that the approach to the asymptotic limit is much faster for larger N. Figure 3 shows the rigidly joined case. The rise in r is much slower due to the resistance of the joints.

The maximum normalized bending moment occurs at the midpoint of each element. Figures 4, 5 show that the curvature changes in the hinged case are much faster than those in the rigidly joined case. For low N, the rise is slower but the asymptotic values are larger. Figure 6 shows the force at the joints or hoop tension h. Our approximations are very close to the exact numerical results. Figures 2–6 are useful for design purposes.

Figure 7 shows the deformation configurations for the hinged, $N = 3$ case. As the rotation parameter B is increased, the equilateral triangle bulges out due to centrifugal forces. Figure 8 shows the rigidly joined case with much smaller deformations for the same B values. Figure 9 shows the deformations of the hinged six-sided polygon. At $B = 100$ the shape is almost a circle. Figure 10 shows similarly the rigidly joined case. The moment at the corners is opposite but less in magnitude than the moment at the midpoints.

Our results could also be applied to hollow polygonal cylinders rotating about their symmetry axis instead of polygonal frames constructed from rods. The only difference would be in the flexural rigidity EI.

6. References.

[1] Ashley, H. "Observations on the dynamic behavior of large flexible bodies in orbit," *AIAA J.* **5**, 1967, pp. 460–469.

[2] Wang, C.-Y. "Rotation of a free elastic rod," *J. Appl. Mech.* **49**, 1982, pp. 225–227.

[3] Wang, C.-Y. "Equilibrium configurations and energies of the rotating elastic cable in space," *AIAA J.* **24**, 1986, pp. 2010–2013.

[4] Wang, C.-Y. and Watson, L. T. "Free rotation of a circular ring about a diameter," *J. Appl. Math. Phys.* **34**, 1983, pp. 13–24.

[5] Watson, L. T. and Wang, C.-Y. "Free rotation of a circular ring with an unbalanced mass," *AIAA J.* **27**, 1989, pp. 1650–1652.

[6] Moré, J. J., Garbow, B. S., and Hillstrom, K. E. *User Guide for MINPACK-1*, ANL-80-74, Argonne National Laboratory, 1980.

[7] Watson, L. T., Billups, S. C., and Morgan, A. P. "HOMPACK: A suite of codes for globally convergent homotopy algorithms," *ACM Trans. Math. Software* **13**, 1987, pp. 281–310.

[8] Watson, L. T. "A globally convergent algorithm for computing fixed points of C^2 maps," *Appl. Math. Comput.* **5**, 1979, pp. 297–311.

[9] Watson, L. T. "Numerical linear algebra aspects of globally convergent homotopy methods," *SIAM Rev.* **28**, 1986, pp. 529–545.

[10] Watson, L. T. and Scott, L. R. "Solving Galerkin approximations to nonlinear two-point boundary value problems by a globally convergent homotopy method," *SIAM J. Sci. Stat. Comput.* **8**, 1987, pp. 768–789.

[11] Heruska, M. W., Watson, L. T., and Sankara, K. K. "Micropolar flow past a porous stretching sheet," *Comput. & Fluids* **14**, 1986, pp. 117–129.

[12] Dennis, J. E. and Schnabel, R. *Numerical Methods for Unconstrained Optimization and Nonlinear Equations*, Prentice-Hall, Englewood Cliffs, NJ, 1983.

Figure Captions

Figure 1. a) The rotating polygonal frame. b) The coordinate system. c) An elemental length.

Figure 2. Distance from center of mass to midpoint of a side, hinged case. Dashed lines are approximations (42) or (49).

Figure 3. Distance from center of mass to midpoint of a side, rigidly joined case. Dashed lines are approximations (42) or (49).

Figure 4. Maximum normalized moment, hinged case. Dashed lines are from Equations (43) or (49).

Figure 5. Maximum normalized moment, rigidly joined case. Dashed lines are from Equations (43) or (49).

Figure 6. Normalized force at a joint, H. ——— hinged case; —·—·— rigidly joined case. Dashed lines are from Equations (40) or (49).

Figure 7. Deformations for $N = 3$, hinged case.

Figure 8. Deformations for $N = 3$, rigidly joined case.

Figure 9. Deformations for $N = 6$, hinged case.

Figure 10. Deformations for $N = 6$, rigidly joined case.

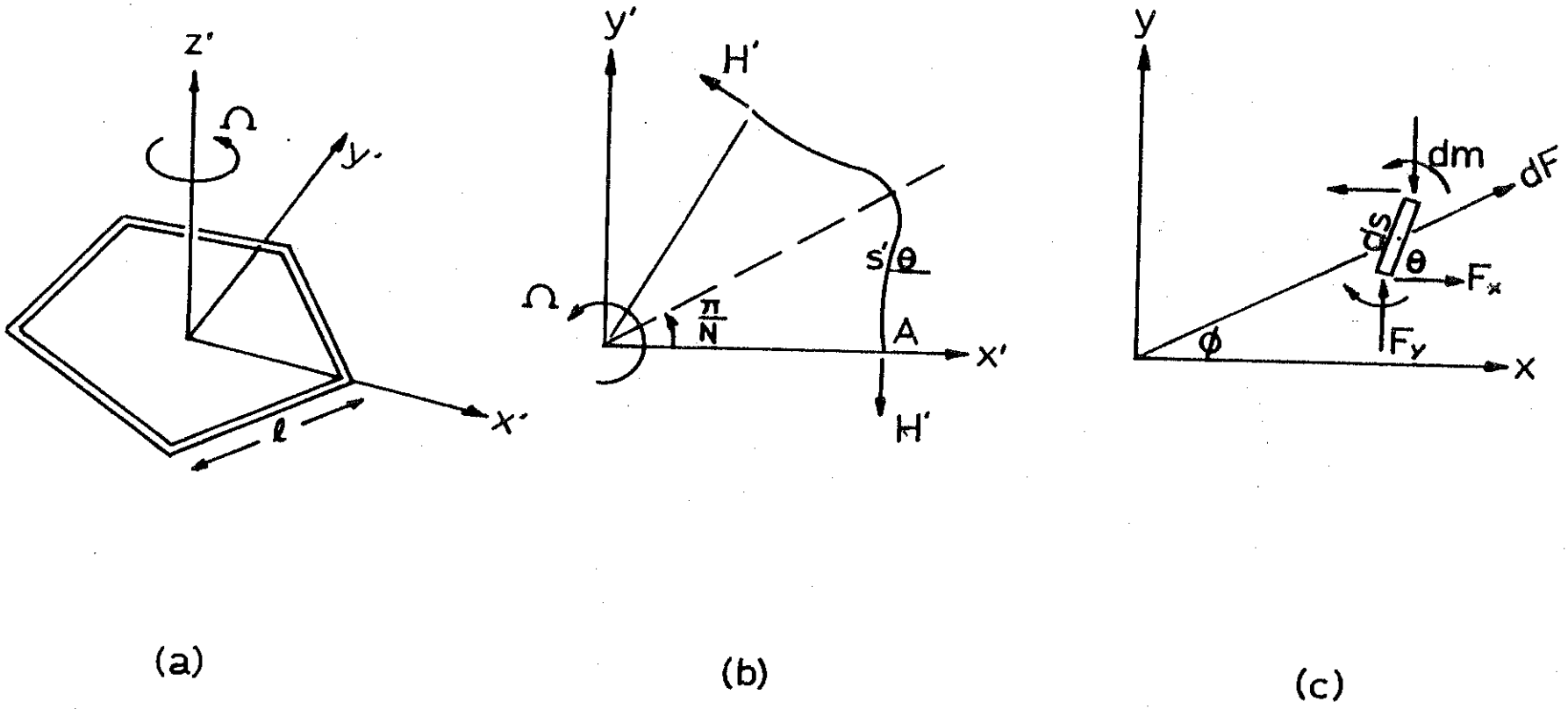

Fig 1

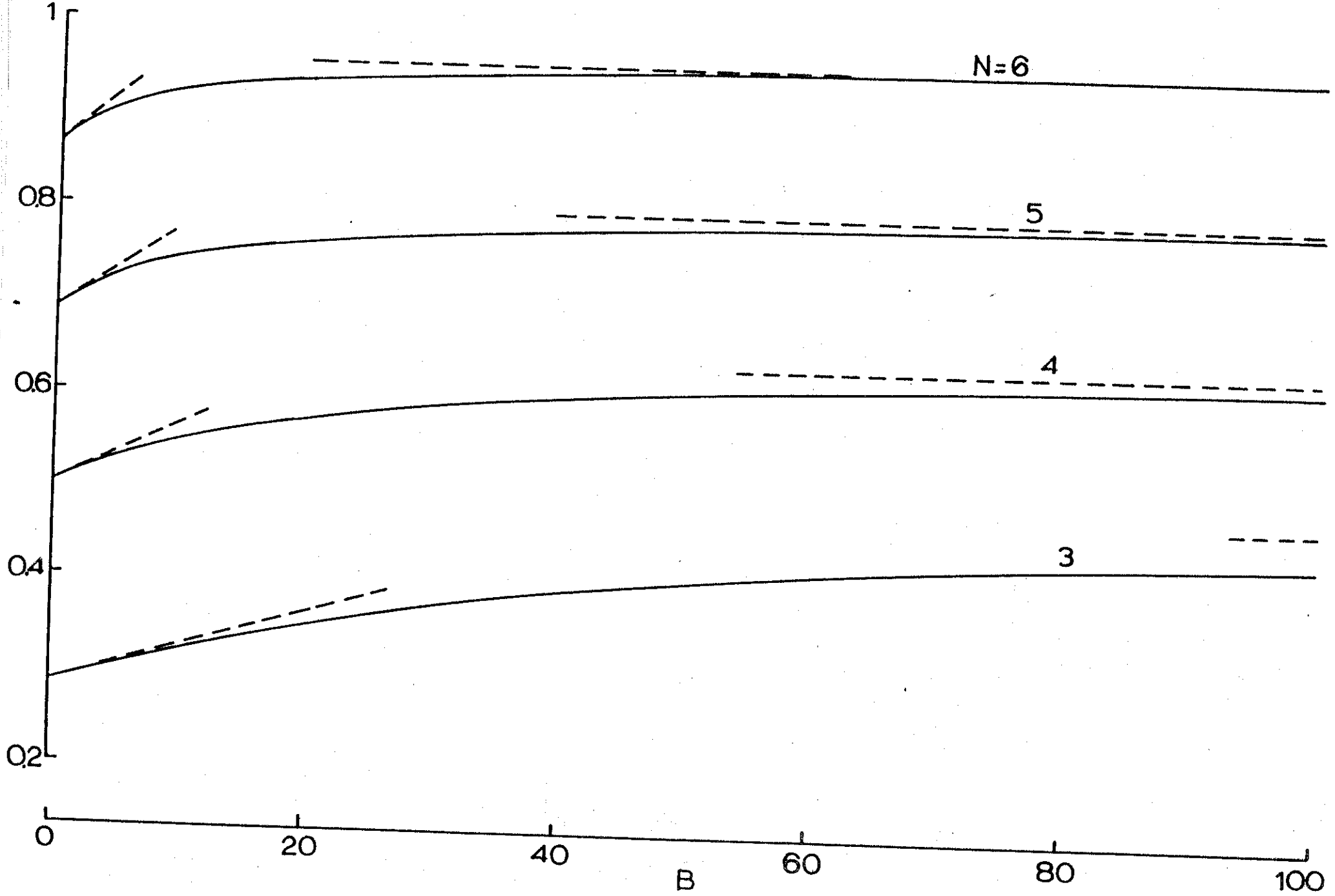

Fig 2

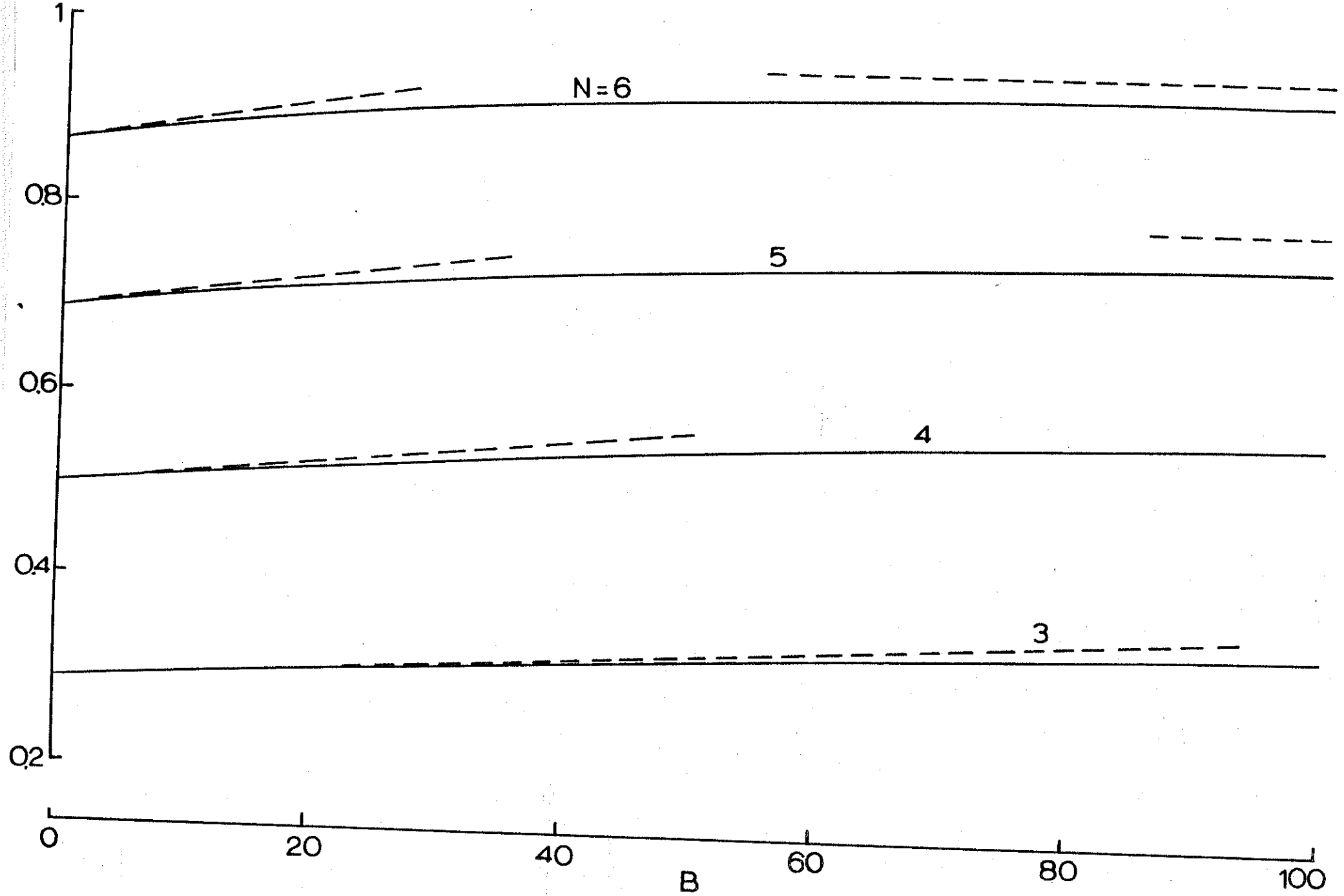
1
0.8
0.6
0.4
0.2
N=6
5
4
3
0
20
40
60
80
100
B

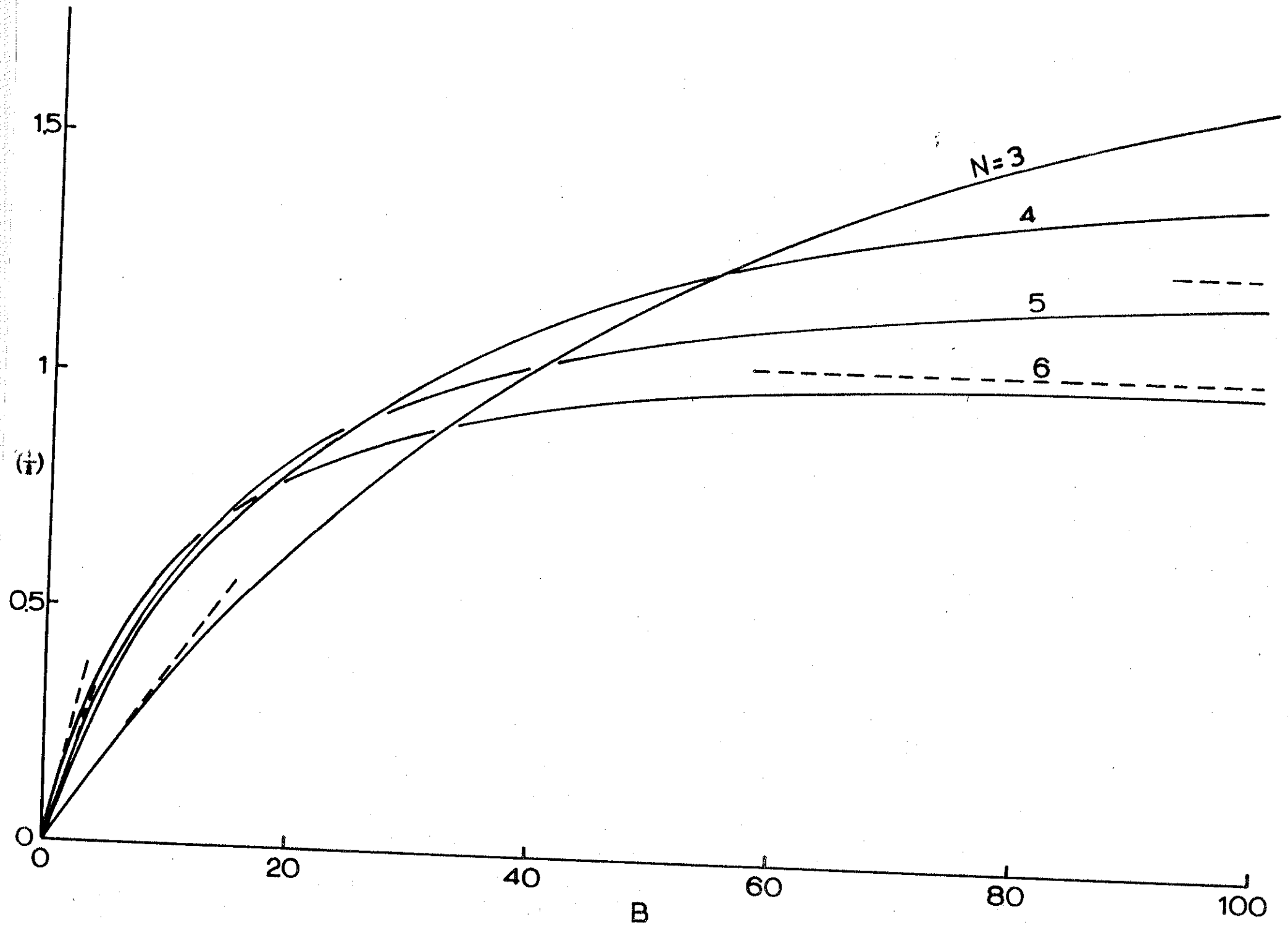

Fig 1

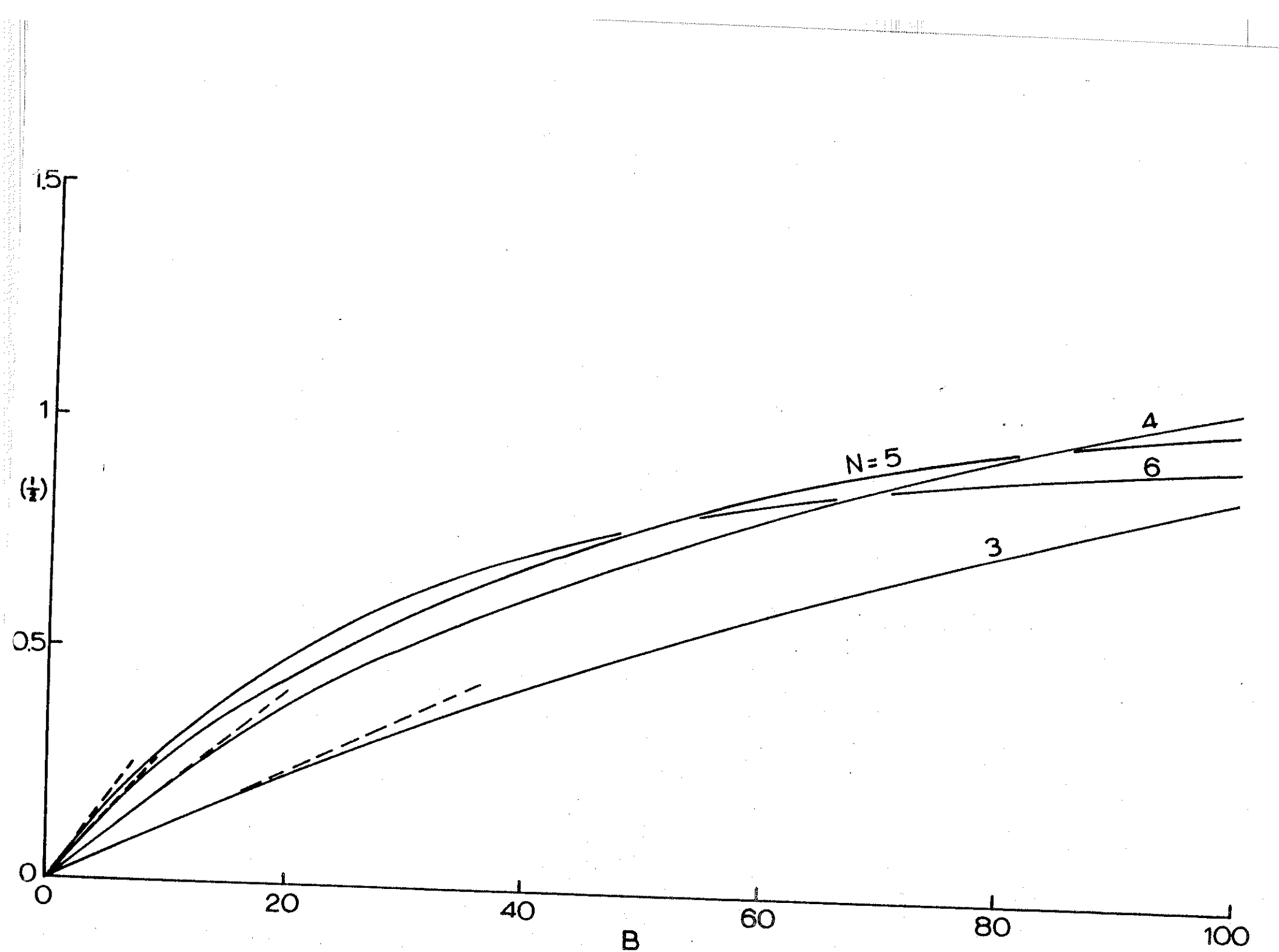
1.5
1
0.5
0
(1/2)
N=5
4
6
3
0
20
40
60
80
100
B

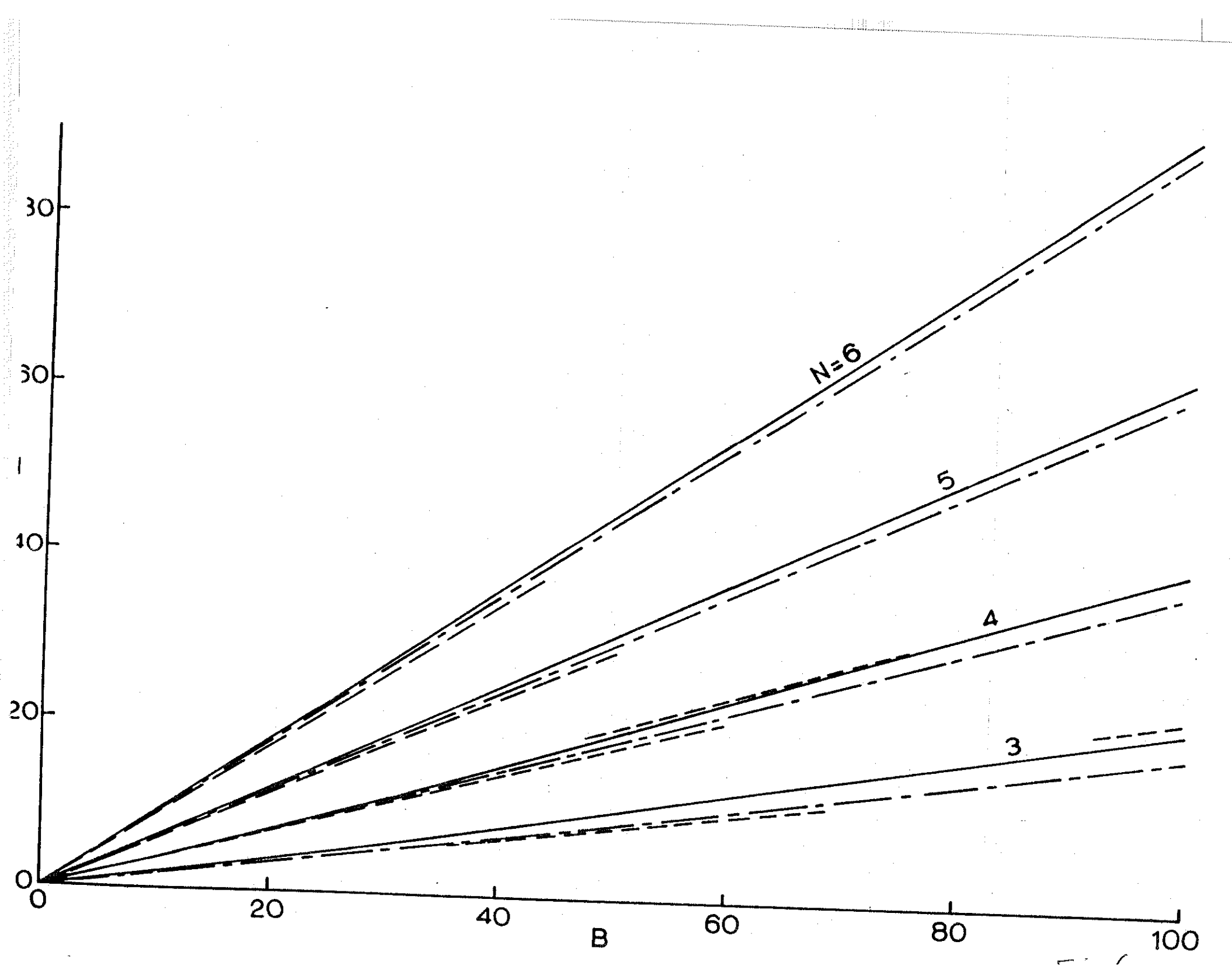
30
30
1
40
20
0
0
20
40
60
80
100
B
N=6
5
4
3

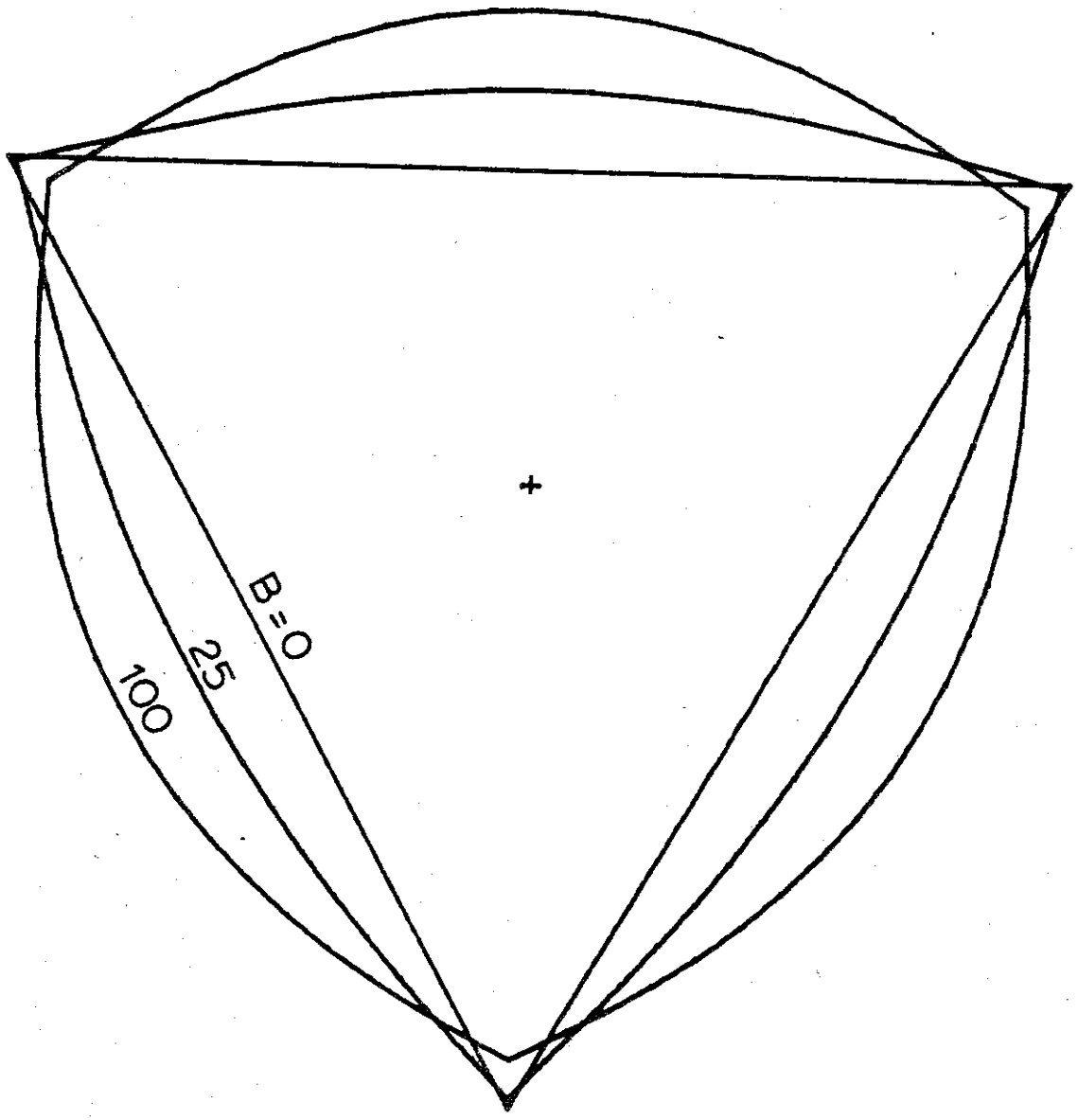
B=0
25
100

Fig 8

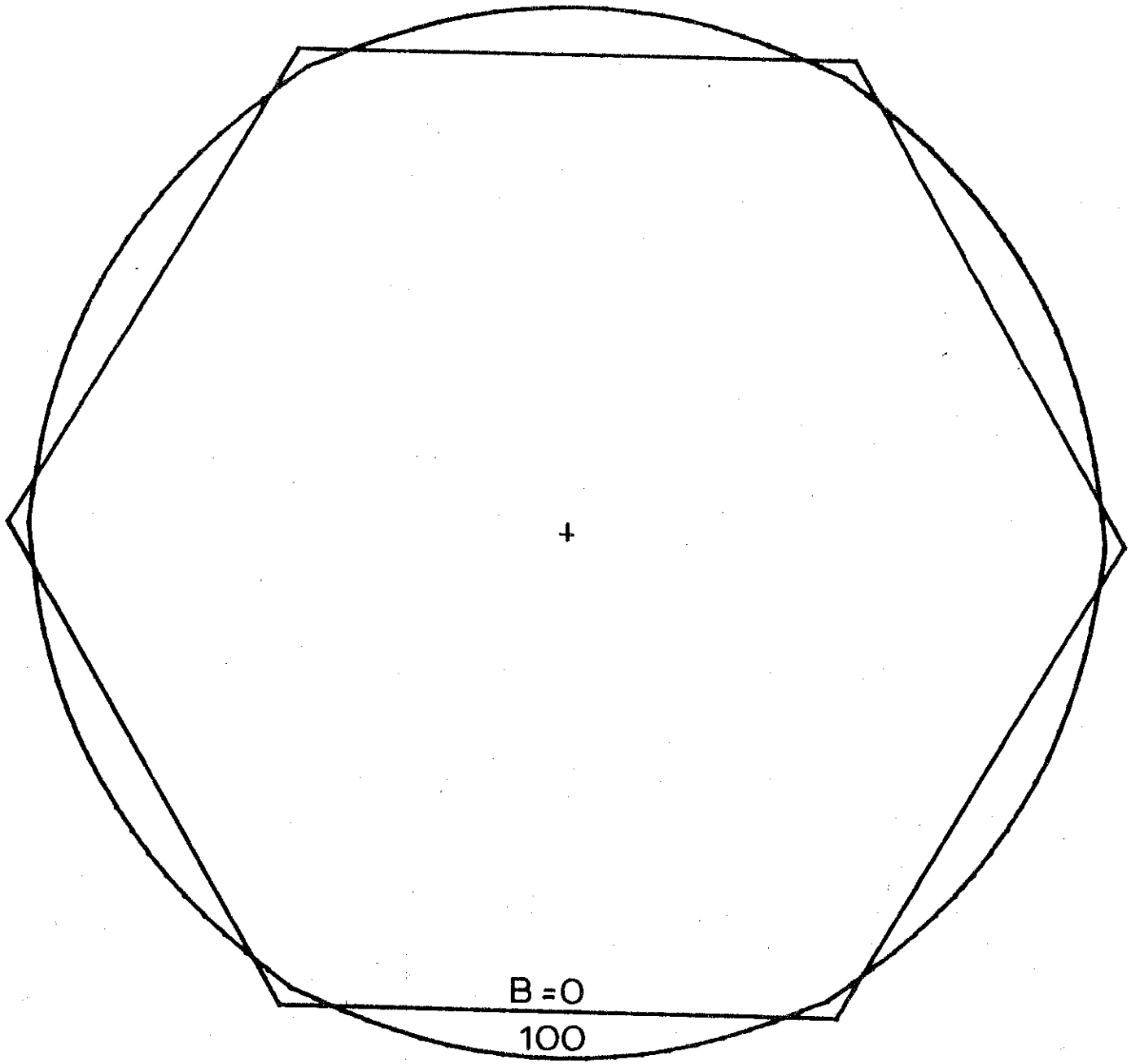

Fig 2

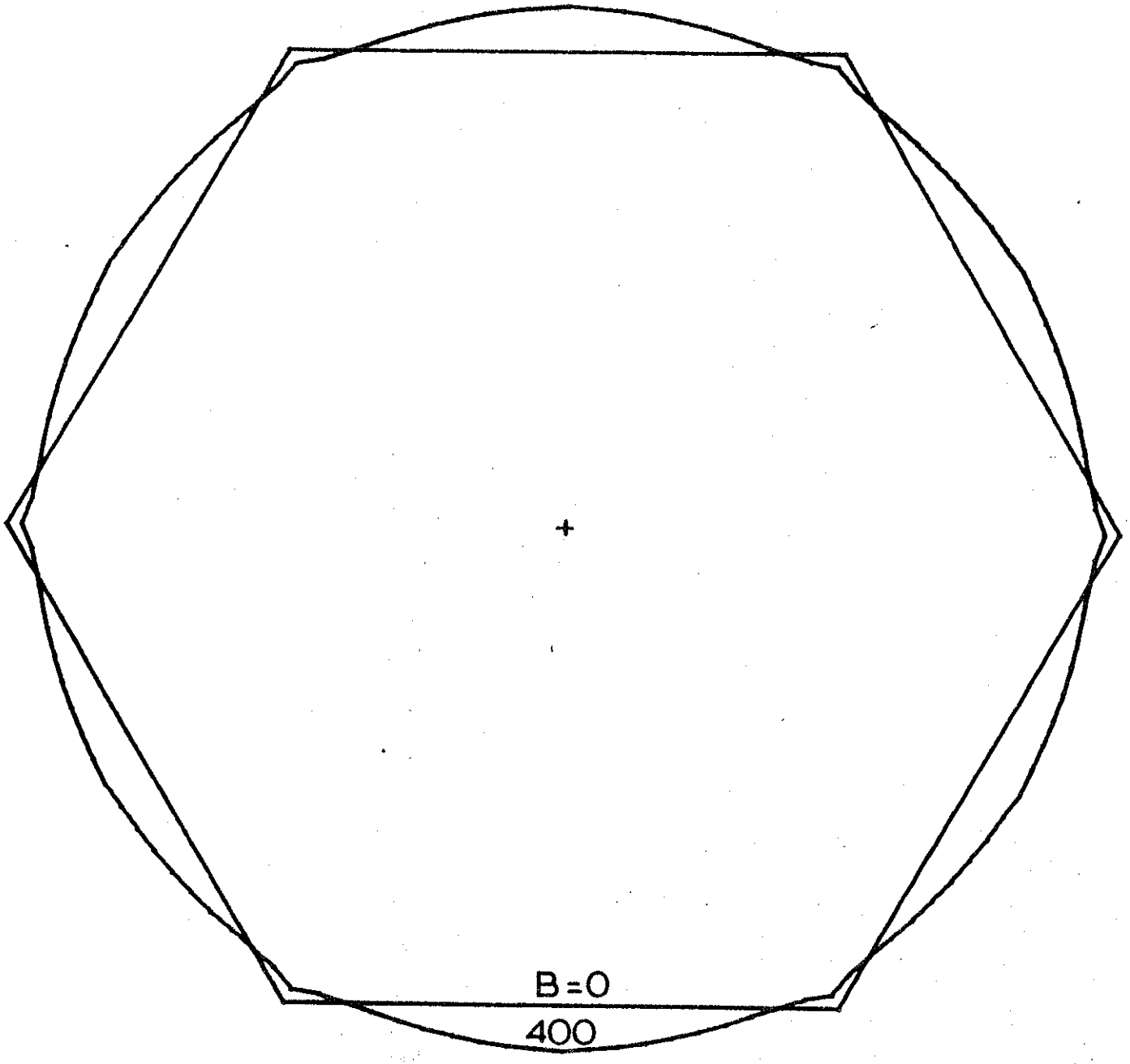

Fig 10